

N71-29923

**NASA TECHNICAL
MEMORANDUM**

NASA TM X-62,028

NASA TM X-62,028

UNIPOLAR INTERACTION OF MERCURY WITH THE SOLAR WIND;
THE STEADY STATE BOW SHOCK PROBLEM

D. S. Colburn, C. P. Sonett, and K. Schwartz

Ames Research Center
Moffett Field, Calif. 94035

**CASE FILE
COPY**

July 1971

UNIPOLAR INTERACTION OF MERCURY WITH THE SOLAR WIND;
THE STEADY STATE BOW SHOCK PROBLEM

D. S. COLBURN and C. P. SONETT

Ames Research Center, NASA

Moffett Field, California 94035

and

K. SCHWARTZ

American Nucleonics Corp.

Woodland Hills, California 91364

ABSTRACT

The steady state electromagnetic interaction of the solar wind with the planet Mercury is computed for a spectrum of electrical conductivity functions using the assumption that no atmosphere or magnetic field damps the direct interaction. The form of the induction is described by the unipolar effect and corresponds to the zero frequency limit of a transverse magnetic (TM) mode. Calculations are included to determine the effective surface temperature of the planet. These calculations include the apparent motion of the Sun in the Hermean sky. It is shown that a significant interaction, detectable by a space probe, is plausible for reasonable conductivity functions. The strength of the interaction is considered in terms of the subsurface thermal gradient, and computations are given relating the strength of the solar wind interaction with the conductivity parameters.

1. Introduction

The electromagnetic field in the solar wind as viewed from a planet is resolvable into two components, the transverse magnetic (TM) and the transverse electric (TE). The TM component is driven by the motional electric field, $\underline{E}_m = \underline{v} \times \underline{B}$ where \underline{v} is the bulk vector velocity of the planet with respect to the solar wind and \underline{B} the interplanetary magnetic field, while the TE component is driven by $\dot{\underline{B}}$, the time variation of the magnetic field [1,2]. The response of the planet to this electromagnetic field can similarly be decomposed into the TM and TE components. The TM mode has a peak response at zero frequency (the steady state) and can be responsible for formation of a steady state magneto-hydrodynamic shock wave. The response of this mode decreases with frequency, asymptotically approaching zero with increasing frequency. The TE mode displays a complementary response, rising from zero in the steady state to a value determined by the constitutive parameters of the combined system formed by the solar wind and the planet.

In both cases the net electromagnetic forcing function driving the planetary response may be decreased because of magnetohydrodynamic effects that tend to deviate the flow to the limbs of the planet. In the limit of a strong interaction, a shock wave will form and then, except perhaps for singular geometries, only approximations to analytic solutions can be obtained.

Extended discussions of the interaction phenomenon have been given in the literature; the case of the Earth is most exhaustive, the Moon has been treated to some extent [1,2,3,4], while planets such as Mars and Venus are still under investigation [5]. Ness and Whang [6] have recently studied the case of Mercury.

Sonett and Colburn [4] have suggested a division of the possible planetary interactions into three major categories. Those planets endowed with a strong internal dynamo-generated planetary magnetic field capable of standing off the solar wind are of Type I, while those planets devoid of either such a magnetic field or atmosphere permitting direct surface contact by the solar wind fall into Type II. Type III planets are those with only an atmospheric interaction. Alternatively, these may be identified as magnetospheric (Earth and Jupiter), geospheric (Moon, Mercury, and perhaps the asteroids) and lastly anemospheric (Mars and Venus) where some evidence exists for an interaction of the solar wind with the atmosphere of the planet.

In the case of the Moon no evidence has yet been found for a steady state interaction [7-11] suggesting that the TM mode response is very weak. On the other hand the response of the Moon to time dependent changes in the interplanetary field is exceptionally strong, showing that the TE mode is important [12-15]. These conclusions for the Moon indicate that the crustal electrical conductivity, which dominates the TM mode response is low, while the internal conductivity, important in the TE mode response, is quite large.

If the planetary interaction is weak, the TE and TM modes can be separated. In the strong interaction where a shock wave develops, the two modes are linked magnetohydrodynamically and the current systems are coupled through the fluid motion on the exterior. The flow field for the weak steady state lunar interaction has been treated by Spreiter et al. [16], and is assumed separable from the interior problem that is solved using conventional electromagnetic theory.

The response of the Moon to the interplanetary magnetic field in the TE mode suggests that a similar interaction may take place at Mercury, which appears to be devoid of either a dynamo field or detectable atmosphere. Since only the total magnetic field, i.e., the sum of the forcing function and the response is determined by a single spacecraft, it is difficult to separate effects due to the TE mode. On the other hand the detection of a steady state unipolar interaction (the low frequency limit of the TM mode) can be made by a single space probe. Inferences can then be drawn regarding the crustal conductivity. Ness and Whang [6], employing a two-layer model of Mercury have concluded that the conductivity of the outer layer is probably too low to produce a detectable solar wind deflection, although they do not rule out such an interaction. However, for the continuously varying conductivity profiles used here and for a large class of silicate materials, measurable solar wind deflection is anticipated.

The calculations made in this paper are aimed at finding the combination of thermal profile and bulk electrical conductivity leading to a detectable steady bow shock wave on Mercury. Only the low frequency limit of the TM mode is employed. The connection between this mode and the formation of a shock wave is known to depend on the flow of a current system through the planet closing in the solar wind in the manner of a linear unipolar generator, i.e., current loops are forbidden to close in the planetary interior [3,4].

We employ as a figure of merit for the presence of a shock wave, a pure number k ($0 < k < 1$), which defines the fraction of the incident solar wind flow deflected to the limb of the planet. While the interaction of the solar wind with a TM planetary current system is extremely complex and the details have not been

worked out, the k factor concept has been useful in previous analyses [3,4,11,17, 18] to outline a necessary transition between two extremes: a weak interaction in which the generated magnetic pressure is proportional to the motional electric field in the solar wind, and a very strong interaction in which the magnetic pressure cannot be expected to exceed that required to completely deflect the solar wind. For values of k below a certain bound it is assumed that a shock wave would be too weak for detection by the conventional means of magnetometer and plasma probe. The basic calculations follow the earlier one of Schwartz et al. [11] in the search for a weak lunar limb shock wave. The thermal models on which the calculations rest are based on solutions to the heat conduction equation using appropriate best estimates for radioactive heat sources with their outward movement caused by the differentiation of silicates. The models are restricted to solutions of the time history problem since no actual measurements are available. The planetary composition, including the presumed high iron content, leads to concentrations of radionuclides substantially different from those of the Earth.

In the subsequent sections we discuss first the details of the thermal models and then the assumed surface temperature, which is a crucial factor in the assessment of the strength of the interaction. The results of the model calculation are then discussed and related to expressions for the dependence of the bulk electrical conductivity upon the temperature of some representative planetary matter. The available power in the solar wind is also discussed as a possible limitation to the interaction.

2. Thermal models of Mercury

Calculations of the solar wind planetary interaction are based on two thermal profiles obtained by Fricker and Reynolds [19] representative of the wide range of uncertainty regarding the temperature of the deep interior. The numerical methods employed follow the outline given by Fricker et al [20]. The internal structure is based on the calculations by Reynolds and Summers [21]. One is a "warm" model with core temperature of 1017° C, based on an initial temperature of 400° C and an initially uniform distribution of radioactives. The other is a "hot" model with core temperature of 2070° C based on a higher initial temperature and a concentration of radioactive heat sources near the surface.

The surface temperature shown in these models is 175° C, obtained by the solution of the black body equation (next section). The surface temperature is not critical for the generation of the thermal models, which depends largely on the solution of the thermal conduction equation. The Fricker and Reynolds models have been modified here to obtain a different surface temperature. The revised models are still considered representative of hot and warm models of Mercury since the revision does not substantially affect the deep internal temperature. The two revised profiles are given in fig. 1, in which the temperature is plotted vs. the radial distance from the center of the planet.

Fig. 1

Majeva [22] has also calculated a thermal profile of Mercury based on thermal history calculations. An initial temperature of 1000° K is assumed based on accretion. The present time profile has an interior temperature of

approximately 2100° K decreasing to about 700° K on the surface. Except for the surface temperature, this is similar to the Fricker and Reynolds hot model.

Radioactive concentrations in this model are those compatible with a high iron content, and consequently are lower than those based on other materials.

3. Surface temperature of Mercury

The primary factors in determining the temperature of the sunlit side of Mercury are the heat input from the Sun and the radiation loss into space, since the effects of conductivity and of thermal inertia are less by orders of magnitude. Soter and Ulrichs [23] have calculated temperature vs. time plots for various points on the Hermean equator that are due to a rotation period 2/3 of the orbital period. The temperature of a point on the equator reaches a high of about 650° K at local noon, and at sunset plunges to a value of approximately 150° K that depends on assumptions about the thermal conductivity, density and heat capacity of the material. Because of the subsynchronous spin period and the elliptic orbit, different points on the equator reach different noontime temperatures, in the range of 570° to 700° K, and the shapes of the temperature-time profiles are different because of the apparent retrograde periodic motion of the sun in the Hermean sky.

The surface temperature is calculated by balancing the heat received and the heat radiated per unit area. The insolation is given by

$$H_i = fr_e^2 \cos \theta / r^2 \quad (1)$$

where r is the instantaneous solar distance, $r_e = 1$ AU, θ is the angle between the Sun line and the zenith and $f = 1388$ Joules/m² sec, the solar constant. The thermal radiation loss is given by

$$H_0 = \epsilon \sigma T^4 \quad (2)$$

where T is the local surface temperature, $\sigma = 5.669 \times 10^{-8}$ Joules/m² deg⁴ sec is the Stefan-Boltzmann constant and $\epsilon = 1$. In eq. (2) the background temperature is considered low enough to be negligible. Solving for the temperature, we obtain

$$T = \left(f r_e^2 \cos \theta / \sigma r^2 \right)^{1/4} \quad (3)$$

Using extreme values of 0.31 and 0.47 for r/r_e the respective temperatures are 710° and 577° K, in agreement with Soter and Ulrichs. The function $(\cos \theta)^{1/4}$ is relatively flattopped, so that temperatures tend to stay high during most of the day.

During the night the surface heat balance is between radiated heat and heat conducted out to the surface from the subsurface layer. The conduction process occurs also during the day but at a negligible rate with respect to solar input or daytime radiative loss. Calculation of the nighttime temperature involves the selection of values for density, conductivity, and heat capacity of the surface material. Instead we rely on the interpretation of recent microwave observations by Chase et al. [24] implying an equatorial midnight temperature of 110° ± 15° K. These workers also find a drop of 10° between midnight and dawn that we neglect

because its effects would tend to average out when obtaining a mean temperature. Murdock and Ney [25] using similar methods have determined the average dark-side temperature at $111^\circ \pm 3^\circ$ K.

The surface temperature used in our calculations is based on a time average of the temperature-time profile plotted in fig. 2. In this profile the daytime temperature is obtained by use of eq. (3) and a circular orbit with $r = (0.3829 r_e)$. The nighttime temperature is taken to be steady at 110° K. Since thermal conduction is linear, the subsurface temperature is an average of the curve in fig. 2 or

Fig. 2

$$T_{av} = \frac{1}{2\pi} \left[110 \pi + 2 \int_0^{\pi/2} 639.3 (\cos \theta)^{1/4} d\theta \right] \quad (4)$$

The integral is evaluated by means of gamma functions giving $T_{av} = 330^\circ$ K (57° C).

The temperature of a black body at Mercury's orbit is more than 100° higher than the average temperature based on a time average of surface temperature.

By using arguments based on expected thermal properties of the Hermean surface, we show in the next section that the thermal wave oscillation for the 176-day period penetrates to a depth of a few tens of meters at most. A mean temperature of 75° C has been arbitrarily selected for calculations for the rest of this paper. Numerical calculations are also made for a lower bound temperature of 50° C and an upper bound of 100° C. Interpolation of the results can be made for any temperature within the range $50^\circ \leq T \leq 100^\circ$ C, which brackets the 57° C temperature estimated above.

For a more complete definition of surface thermal models of Mercury refer to Morrison and Klein [26] who use microwave measurements and discuss the increase of temperature with depth and the temperature dependence of thermal conductivity. These and other parameters make the surface temperature estimate of 75° C preliminary but we adopt it to illustrate the electromagnetic interaction of Mercury with the solar wind.

4. Thermal properties of the skin layer

The electrical conductivity of the surface layer plays a dominant role in the electrical induction calculations to be shown later. In this section we obtain an estimate of the depth below which the temperature profile is unaffected by solar heating and radiative cooling during the synodic rotation period. This depth is of the order of 10 m.

Because the thickness of the layer in which time variations are significant is a small fraction of the radius, a one-dimensional geometry is appropriate. The cyclic variation of the temperature at the surface can be Fourier analyzed. Because the skin depth of the fundamental component is greater than those of the harmonics, however, only the fundamental will be retained in the following discussion. The surface temperature then has a time dependence of the form

$$T = T_0 \cos(\omega t) \quad (5)$$

where T_0 is the difference between noon and midnight temperatures and $\omega = 2\pi/176$ days is the synodic rotation rate. The solution for the temperature wave in the interior can be shown to be of the form

$$T(x,t) = T_0 \exp(-x/\sigma) \cos(\omega t - x/\sigma) \quad (6)$$

where x is the depth. The skin depth, σ , is defined by $\sigma^2 = 2\alpha/\omega$, where α is the thermal diffusivity, i.e., the ratio of thermal conductivity to the product of density and specific heat. At π skin depths, the phase of the thermal wave is inverted and the amplitude decreases to only 0.043 of the surface value. For $\alpha = 10^{-6} \text{ m}^2/\text{sec}$, $\sigma = 2.2 \text{ m}$. Thus even for the extremely slow orbital frequency of Mercury the bulk electrical conductivity oscillates significantly only in a layer of thickness less than 10 m. On the day side this layer operates as an electrical short circuit of negligible thickness. On the night side the layer may present significant resistivity if a pure extrapolation is made from the electrical conductivity functions described in the next section. We assume that local inhomogeneities will allow the current to cross the extremely thin layer of temperature cycling so that the planet can be treated electrically as having a time stationary temperature profile.

5. Conductivity functions

In model calculations of the planetary electromagnetic response, the electrical conductivity is analytically represented by a function of the form

$$\sigma = \sum_{i=1}^3 \sigma_{0i} \exp\left(-\frac{E_i}{\eta T}\right) \quad (7)$$

where $\sigma(T)$ is the electrical conductivity, T is the temperature, E the activation energy, η Boltzmann's constant, and σ_0 the conductivity at $T = \infty$, essentially

a mobility-like term that depends on the detailed quantum statistics of the material. Only the term for $i = 1$ is applied in calculating the steady electromagnetic response of Mercury. The justification for omitting the other terms is that the low temperature outer layers of the planet are dominant in determining the response, and at these temperatures impurity semiconduction plays the primary role. For possible crustal compositions σ_0 may vary widely and E tends to fall within the general range of 0.5 to 0.8 eV. To cover the range in the calculations we use $E = 0.5$ and 0.8 eV and in each case let σ_0 vary over a wide range. As one approaches the deep interior of the planet the conductivity function might change. However, the change is not important in these calculations because generally the interior temperature is elevated sufficiently to cause the core to act like an electrical short circuit, making the exact form of the conductivity function unimportant.

Table 1 shows values of σ_0 and E for various candidate materials. The list is a representative fraction of the determinations made by various groups, and for each material there are a variety of estimates. The range of values is expected to encompass the parameter combination suitable for Mercury, and the materials in the table will be compared in the ensuing calculations.

Table 1

Electrical conductivity function parameters

Symbol	Material Name	σ_0	E	Reference
O ₁	Olivine	0.016	0.66	[27]
O ₂	Olivine	1.0	0.64	[28]
O ₃	Olivine	0.01	0.5	[29]
O ₄	Olivine	200	0.92	[30]
P ₁	Peridotite	3.2	0.8	[27]
P ₂	Peridotite	3.8	0.81	[31]
D ₁	Diabase	160	0.68	[27]
D ₂	Diabase	10 ³	0.63	[27]
D ₃	Basalt Diabase	130	0.78	[27]
M	Lunar Sample 10024.22	7.6	0.5	[32]

6. Current density

In the unipolar generator calculation the motional electric field driving the current system is the $\underline{v} \times \underline{B}$ field resulting from the solar wind velocity and the interplanetary magnetic field whose average direction lies along the Parker spiral angle. The numerical value of the field is $vB_\phi = \omega r B_r$, where ω is the solar spin, r the solar distance and B_r the radial component of the interplanetary field. For these calculations $B_r = 7$ gamma at 1 AU from the Sun and is correspondingly greater at the orbit of Mercury since it varies

as r^{-2} . The solar wind is assumed to have a velocity of 400 km/sec at the Earth and at Mercury; the number density of $10/\text{cm}^3$ is increased to $66.8/\text{cm}^3$ at the nominal orbital distance of Mercury, 0.387 AU.

As in our earlier calculations the temperature is assumed to have a well-behaved dependence on only the planetary radius. It follows, therefore, that for a spherically stratified body the conductivity function depends solely upon radius. We calculate first the current densities in the planet to illustrate the effect of changing temperature. The fundamental equation determining the electric potential is given by

$$\nabla^2 \phi = \frac{\nabla \sigma}{\sigma} \cdot \nabla \phi = 0 \quad (8)$$

which has the form of Poisson's equation and the term

$$\frac{\nabla \sigma}{\sigma} \cdot \nabla \phi$$

represents a charge density, a result of the gradient in the conductivity function, provided that $\nabla \sigma \cdot \nabla \phi \neq 0$, as expected for reasonable cases. The current density is found from

$$I = \sigma E = -\sigma \nabla \phi$$

and integrated to find the total current. Sample calculations are carried out for both warm and hot models of Mercury, using three values of the subsurface temperature T'_s (the temperature at a point under the surface at a distance sufficient to damp out the thermal insolation wave). For both models the activation energy, E , is set equal to 0.5 and 0.8 eV. The resultant current densities are given in

table 2. There the quantity, σ , is varied in two different but related ways. The column designated ($\sigma_s = 1$) covers cases where the model is scaled so that for convenience the subsurface conductivity is unity irrespective of T_s' . The adjustment is made by changing the value of σ_0 so that the subsurface conductivity, σ_s , attains the fixed value of 1 mho/m. Thus the temperature dependence of the conductivity function is retained, the effect showing in the small variation of current density with change in T_s' . The columns labeled ($\sigma_{75} = 1$) show the current density for cases where the subsurface conductivity itself is permitted to vary with temperature; here the base value of 1 mho/m was set arbitrarily for the temperature case where $T_s' = 75^\circ \text{C}$, and the other two values thus changed accordingly. For actual cases, the total current, I_c , flowing through the equatorial plane is obtained from the number in table 2 (column $\sigma_s = 1$) by using the formula

$$I_c = \pi a^2 \sigma_s i_{AV} = 1.87 \times 10^{13} \sigma_s i_{AV} \quad (9)$$

where $a = 2.44 \times 10^6 \text{ m}$ is the radius of Mercury, i_{AV} is the value taken from table 2 and σ_s the actual value of the electrical conductivity at the surface.

In table 2 the calculations for $\sigma_{75} = 1$ show a large change in the current density when the surface temperature increases or decreases by 25° . The changes range from three to seven for a 25° change. This marked effect is caused by the sensitivity of the total electrical resistance of the surface layer to temperature changes in the temperature range of 75°C . In the columns for which the surface conductivity is held fixed ($\sigma_s = 1$) the internal conductivity is

Table 2

Mean planetary current density (amps/m) for various thermal models, activation energies, E, and subsurface temperatures, T'_s , normalized to unity subsurface current density.

Model	Activation Energy, E (volts)	Subsurface Temperature, T'_s (C)		
		50	75	100
Hot	0.5	8.81	2.42	7.44
	0.8	15.2	1.93	12.97
Warm	0.5	1.44	0.40	1.22
	0.8	2.47	0.31	2.11

Calculated current densities do not include the effects of saturation, i.e., the k factor.

($\sigma_s = 1$) ($\sigma_{75} = 1$) ($\sigma_s = 1$) ($\sigma_{75} = 1$) ($\sigma_s = 1$) ($\sigma_{75} = 1$)

19.4

67.1

3.18

10.9

somewhat higher for the lower surface temperature cases since the conductivity increases with depth more rapidly for the surface temperature of 50° C than for the 75° case or the 100° case. The variations, however, are much smaller, of the order of 0.8% per degree. This increase is directly related to an increase in the slope of the conductivity function with depth. A much larger change occurs as the activation energy is changed from 0.5 to 0.8 eV. This too produces a change in the slope of the conductivity. The largest variation occurs between the warm and hot models, a factor of 6. In this case it is the steepness of the temperature profile itself that causes the derivative of the conductivity function to change.

Sonett and Colburn [3] have shown that for a strong interaction, a saturation takes place where the magnetic field from the induction is sufficient to deflect a substantial fraction of the incoming solar wind to the flanks of the planet. In that instance, the available motional electric field is reduced and the final value of induction is determined by the joint action of the induction and the deflection of the flow. The fraction of the flow field deviated is defined by a pure number k where $0 < k < 1$.

To obtain a meaningful result the k factor limitation must be applied to the currents obtained from table 2. The actual current, I_a , flowing through the equatorial plane is obtained by the balance of magnetic pressure and the pressure of that portion, k , of the solar wind that is deflected by the current system, or

$$\frac{\mu I_a^2}{8\pi^2 a^2} = knmv^2 \quad (10)$$

where μ is the permeability, m is the mass of a proton, and mks units are used. While the effect of solar wind deflection on the current system is extremely complicated, it is assumed for the first order approximation that the actual current I_a is related to the calculated current I_c by the relation

$$I_a = (1 - k)I_c \quad (11)$$

since the current can be generated by the motional field of only that portion of the solar wind that is allowed to penetrate to the planetary surface.

For the nominal solar wind parameters at Mercury a maximum actual current may be obtained from eq. (10) by setting $k = 1$;

$$I_{\max} = 2\pi av(2nm/\mu)^{1/2} \quad (12)$$

so that at Mercury

$$I_{\max} = 2.585 \times 10^6 \text{ amperes} \quad (13)$$

and the calculated and actual currents are related by

$$I_c = \frac{k^{1/2}}{1 - k} I_{\max} \quad (14)$$

We arbitrarily designate $k = 0.1$ as the threshold value below which the solar wind deflection cannot be detected from a spacecraft. Using eq. (14) the current required for $k = 0.1$ is calculated and applied to the results of table 2

to obtain the surface conductivity required in each case to cause the threshold interaction. The results are shown in table 3, where a value is given for $\log_{10} \sigma_s$ for all of the cases. The conductivities are inversely proportional to the currents of table 2, but the logarithmic tabulation indicates more clearly the relationships between the various cases. Table 3 shows that if a k factor of 0.1 is observed the surface conductivity must be approximately 10^{-8} mho/m for a hot or warm planet or 10^{-5} mho/m for the less likely case of a uniform temperature planet. As surface temperature varies 25° $\log_{10} \sigma_s$ varies 0.07. As activation energy varies 0.3 eV, $\log_{10} \sigma_s$ varies 0.24. As the model changes from the hot to the warm model, $\log_{10} \sigma_s$ varies 0.79.

Table 3

$\log_{10} \sigma_s$ (mho/m) for different models and values of E and $T_s \cdot \sigma_s$ is surface conductivity in mho/m for which $k = 0.1$, i.e., the value for which there will be a perceptible interaction. Thus for the expected cases, a k factor of 0.1 implies a surface conductivity on the order of 10^{-8} .

		$\log_{10} \sigma_s$		
		T = 50 C	T = 75 C	T = 100 C
Hot model	E = 0.5	-8.26	-8.19	-8.12
	E = 0.8	-8.50	-8.43	-8.36
	E = 0.5	-7.47	-7.40	-7.33
Warm model	E = 0.8	-7.71	-7.64	-7.58
Uniform model			-5.18	

In fig. 3 the results of table 3 are generalized to give σ_s for any k factor. The k factor is plotted against σ_s for each case. All the curves have the same shape since σ_s is proportional to $k^{1/2}/(1 - k)$. The intersections of the curves with the $k = 0.1$ line are the values of table 3. For values of k less than 0.1, σ_s drops essentially 0.5 order of magnitude for each order of magnitude of k.

Fig. 3

7. Relation of surface conductivity to σ_0

For each value of E in eq. (7) there is an associated value of σ_0 , if a surface conductivity and a surface temperature have been determined. The possible σ_0 , E pairs can be related to conductivity estimates of known materials. The following discussion is limited to one surface temperature, $T_s = 75^\circ \text{C}$. In fig. 4 σ_0 is plotted against σ_{75} with E as a parameter. Possible σ_0 , E combinations are also shown in the figure. The three vertical bars indicate the regions where one would expect a k factor of 10^{-3} , 0.1 and 0.4. The width and overlap are produced by variations in the thermal models. While the exact values of the conductivity functions and the rock types associated with them are subject to discussion, they are representative of the range of conductivities expected. A k factor of 0.1 or larger is seen to be a distinct possibility because it corresponds to σ_0 , E pairs bracketed by known conductivity function estimates. In particular the conductivity function for a lunar sample labelled M on the figure, favors a strong reaction.

Fig. 4

8. Approximate model for calculated current

The modification of calculated current by surface conductivity, activation energy, temperature, and temperature gradient can be expressed by a simple

approximation based on the control of the current by a crustal resistance. In this case the crust is defined as a region between the surface and a core of negligible resistivity. Neglecting curvature and approximating the temperature variation by

$$\frac{1}{T} = \frac{1}{T_0} + g (r - a) \quad (15)$$

where g , the gradient of reciprocal temperature at the surface, is evaluated by

$$g = \frac{d}{dr} T^{-1} = -T^{-2} \frac{dT}{dr} \quad (16)$$

We then obtain the resistance R from

$$R = \int_{r_0}^{r_c} \frac{1}{\sigma} dr = \frac{R}{\sigma E g} \Big|_{r_0}^{r_c} \quad (17)$$

At r_c , the core radius, the bracketed quantity is taken to be zero because σ has become large. Then $R = \eta (\sigma E g)^{-1}$ evaluated at the surface and consequently the calculated current should be proportional to

$$-\sigma E T^{-2} (dT/dr)$$

The approximation can be compared to the calculated currents in table 2. First, examine the variation with T^{-2} . As the temperature is raised from 50° to 75° C, T^{-2} increases by a factor of 1.161 and current by 1.177. As the

temperature is raised from 75° to 100° C the corresponding factors are 1.149 and 1.164. This shows the calculated current to follow T^{-2} to within a few percent. For variation with E, the average increase in current as E goes from 0.5 to 0.8 is 1.740, slightly higher than the predicted 1.6. The variation with dT/dr is shown by changing from the warm model, with a gradient of 1.60°/km to the hot model with 8.07°/km. The increase in dT/dr by a factor of 5.04 causes an increase in calculated current by a factor of 6.12, about 20% larger than predicted by the simple model.

9. Available solar wind power

As σ_s is increased over its range, the power absorbed by the planet must go through a maximum. The power is low at very low conductivities where the electric field is essentially constant but the current is cut off by the low conductivity. The power is also low at very high conductivities where current is limited by the k factor, approaching the asymptotic value I_{\max} as shown in eq. (10). For a constant current, an increase in conductivity decreases the power absorbed. The maximum power is of interest only to see if it is larger than the available solar wind power, in which case the model can no longer represent the physical process.

It first can be demonstrated that the power dissipated is 2/3 of the product of the total current and the potential from pole to pole. This is shown by the boundary conditions at the surface. If J_p is the current density at the pole, the current density at any point is $J_p \cos \theta$, where θ is the colatitude with

respect to the pole. The total current I_{tot} is obtained by integrating the current density over the hemisphere so that

$$J_P = I_{\text{tot}}/\pi a^2 \quad (18)$$

The current associated with each element of area $2\pi a^2 \sin \theta d\theta$ goes through a potential drop $\phi = 2 E_{\text{mk}} a \cos \theta$, where $E_{\text{mk}} = E_m (1 - k)$ and $E_m = (v \times B)$. Therefore, the power P is

$$P = \int_A J\phi dA = \int_0^{\pi/2} 4\pi a^3 E_{\text{mk}} J_P \cos^2 \theta \sin \theta d\theta \quad (19)$$

giving

$$P = \frac{2}{3} (2 E_{\text{mk}} a) I_{\text{tot}} \quad (20)$$

To determine the k factor for maximum power, we write eq. (20)

$$P = \frac{2}{3} (2\rho) E_m I_{\text{max}} k^{1/2} (1 - k) \quad (21)$$

whereupon differentiation shows that maximum power occurs for $k = 1/3$, with the factor $k^{1/2} (1 - k) \sim 0.385$.

A power ratio R_{min} can now be calculated that is the ratio of solar wind power to the maximum power drawn by the body, occurring when $k = 1/3$. If

$R_{\min} > 1$, the power available from the solar wind will always be sufficient.

The solar wind power is taken as the kinetic energy flux intercepted by the cross-sectional area of the planet, or

$$P_{\text{sw}} = 0.5 \pi \alpha^2 n m v^3 \quad (22)$$

The maximum power in the planet, P_{max} , is obtained from eqs. (12) and (21), giving

$$P_{\text{max}} = \frac{16 \pi v \rho^2 E_m}{9} \left(\frac{2nm}{3\mu} \right)^{1/2} \quad (23)$$

and

$$R_{\min} = \frac{9v^2}{32E_m} \left(\frac{3\mu mn}{2} \right)^{1/2} \quad (24)$$

A separation of parameters occurs in eq. (24). R_{\min} is independent of the size, conductivity function, and other planetary features. It depends only on the solar wind parameters, i.e., the number density, velocity, and motional electric field. The strongest dependence is on velocity, the weakest on number density. For the solar wind parameters used here, $R_{\min} = 2.87$ so that a reduction in $n^{1/2}v^2$ by that factor may cause power limiting. Through hydromagnetic coupling the planetary cross section may be greater than its geometric cross section; in this sense the threshold is conservative. On the other hand, inefficiency of the coupling may lower the available power. The effect of power limiting will be

that the solar wind must be deflected from the planet at a value of current lower than the k factor limit value.

If power limiting is known to be involved, it is important to determine over what range of k factor values it occurs. Using eqs. (12), (21), (22), and (24), we obtain an expression for the power ratio R_P as the quotient of R_{\min} and a relative ratio R_r depending only on the k factor. Thus

$$R_P = \frac{R_{\min}}{R_r} \quad (25)$$

where

$$R_r = 1.5 (3k)^{1/2} (1 - k) \quad (26)$$

R_r is plotted against k in fig. 5 and is shown to range from 0 at $k = 0$ and $k = 1$ to a maximum of 1 at $k = 1/3$; R_r may also be defined as the relative power absorbed by the planet. This expression for the power ratio is unexpected, for it shows that the power ratio depends on all other planetary parameters only through their effect on the k factor. If the k factor were known no additional information such as the size or the conductivity distribution, would be needed. Figure 5 could then be used to compute planetary solar wind interactions. For a given model R_{\min} is first calculated using eq. (21). Then if $R_{\min} > 1$, there is no power limiting, and if $R_{\min} < 1$, the model is only valid for $R_r < R_{\min}$. Then, from fig. 5 (or eq. (26)), the range of permissible k factors is determined.

10. Conclusion

It has been shown that the unipolar generator mechanism is likely to operate at Mercury if the electrical conductivity of the subsurface material conforms to one of the more highly conducting cases. If a solar wind deflection is observed and a k factor is estimated, it will be possible to determine the range of the surface conductivities. By "surface" we mean a layer to a depth of a few tens of kilometers, beyond which the hotter interior acts like an electrical short circuit. The response of a hot model is a factor of 6 greater than the response of a warm model, so that if other means were found to determine the surface conductivity within less than an order of magnitude, some information might be obtained as to the planet's interior temperature. The solar wind power is expected to be generally sufficient to support the mechanism over any range of the k factor.

It is clear that the TM mode requires that current carriers be supplied between the solar wind and the planet. This can take several forms, the most plausible being based on a combination of photoionization and electron collection from the plasma, where emission takes place on the positive hemisphere and collection on the negative. Other models would include using ions as part of the current system, but the electron model seems easiest to justify. Although calculations are not included here it seems likely that the supply of current carriers would not be a limiting factor in the flow of the currents associated with the TM mode.

Lastly an additional reason is available in support of a hot model for Mercury. The low suborbital resonance suggests that if the planet had once been endowed

with greater spin many higher order resonances would have been bypassed as the spin rate decreased to its present ultimate value. This in turn would imply a strong tidal degradation (which in itself might supply some internal heat). The presence of the existing resonance also suggests that the planet may be triaxial lending support to the idea that convection might be present [33,34,35].

REFERENCES

- [1] G. Schubert and K. Schwartz, A theory for the interpretation of magnetometer data, *The Moon* 1 (1969) 106.
- [2] J. L. Blank and W. R. Sill, Response of the moon to the time-varying interplanetary magnetic field, *J. Geophys. Res.* 74 (1969) 736.
- [3] C. P. Sonett and D. S. Colburn, Establishment of a lunar unipolar generator and associated shock and wake in the solar wind, *Nature* 216 (1967) 340.
- [4] C. P. Sonett and D. S. Colburn, The principle of solar wind induced planetary dynamos, *Phys. Earth Planet. Interiors* 1 (1968) 326.
- [5] J. R. Spreiter, A. L. Summers and A. W. Rizzi, Solar wind flow past non-magnetic planets - Venus and Mars, *Planet. Spa. Sci.* 18 (1970) 1281.
- [6] N. F. Ness and Y. C. Whang, Solar wind interaction with Mercury, *J. Geophys. Res.* 76 (1971) 3136.
- [7] E. F. Lyon, H. S. Bridge and J. H. Binsack, Explorer 35 measurements in the vicinity of the moon, *J. Geophys. Res.* 72 (1967) 6113.
- [8] N. F. Ness, K. W. Behannon, C. S. Scearce and S. C. Cartarano, Early results from the magnetic field experiment on Lunar Explorer 35, *Jour. Geophys. Res.* 72 (1967) 5769.
- [9] C. P. Sonett, D. S. Colburn and R. G. Currie, The intrinsic magnetic field of the moon, *J. Geophys. Res.* 72 (1967) 5503.
- [10] D. S. Colburn, R. G. Currie, J. D. Mihalov and C. P. Sonett, Diamagnetic solar wind cavity discovered behind Moon, *Science* 158 (1967) 1040.
- [11] K. Schwartz, C. P. Sonett and D. S. Colburn, Unipolar induction in the moon and a lunar limb shock mechanism, *The Moon* 1 (1969) 7.

- [12] C. P. Sonett and P. Dyal, The moon: global electromagnetic sounding using the solar wind, *Comments on Astrophysics and Space Physics* (in press).
- [13] C. P. Sonett, P. Dyal, C. W. Parkin, D. S. Colburn, J. H. Mihalov and B. F. Smith, Whole body response of the moon to electromagnetic induction by the solar wind, *Science* (in press).
- [14] C. P. Sonett, D. S. Colburn, P. Dyal, B. F. Smith, G. Schubert and K. Schwartz, Lunar electrical conductivity profile, *Nature*, 230 (1971) 359.
- [15] C. P. Sonett, G. Schubert, B. F. Smith, K. Schwartz and D. S. Colburn, Lunar electrical conductivity from Apollo 12 magnetometer measurements: compositional and thermal inferences, *Proc. Apollo 12 Lunar Science Conf. Geochim. et Cosmochim. Acta, Suppl. 2* (in press).
- [16] J. R. Spreiter, M. C. Marsh and A. L. Summers, Hydromagnetic aspects of solar wind flow past the Moon, *Cosmic Electrodynamics* 1 (1970) 5.
- [17] C. P. Sonett, D. S. Colburn and K. Schwartz, Electrical heating of meteorite parent bodies and planets by dynamo induction from a pre-main sequence T Tauri "solar wind", *Nature*, 219 (1968) 924.
- [18] C. P. Sonett, D. S. Colburn, K. Schwartz and K. Keil, The melting of asteroidal-sized bodies by unipolar dynamo induction from a primordial T Tauri sun, *Astrophysics and Space Science*, 7 (1970) 446.
- [19] P. E. Fricker and R. T. Reynolds, in preparation.

- [20] P. E. Fricker, R. T. Reynolds and A. L. Summers, On the thermal history of the moon, *J. Geophys. Res.* 72 (1967) 2649.
- [21] R. T. Reynolds and A. L. Summers, Calculations on the composition of the terrestrial planets, *J. Geophys. Res.* 74 (1969) 2494.
- [22] S. V. Majeva, The thermal history of the terrestrial planets, *Astrophysical Letters* 4 (1969) 11.
- [23] S. Soter and J. Ulrichs, Rotation and heating of the planet Mercury, *Nature* 214 (1967) 1315.
- [24] S. C. Chase, E. D. Miner, D. Morrison, G. Münch and G. Neubebauer, Final Report of the Infrared Radiometer Experiment Science Instrument Team for the 1973 Mariner Venus/Mercury Mission, (Jet Propulsion Laboratory, Pasadena, 1970).
- [25] T. L. Murdock and E. P. Ney, Mercury: the dark-side temperature, *Science* 170 (1970) 535.
- [26] D. Morrison and M. J. Klein, The microwave spectrum of Mercury, *Astrophys. J.* 160 (1970) 325.
- [27] E. I. Parkhomenko, Electrical Properties of Rocks (Plenum Press 1967).
- [28] K. Noritomie, The electrical conductivity of rocks and the determination of the electrical conductivity of the Earth's interior, *J. Mining Coll. Akita Univ.* 1 (Series A) (1961) 27.
- [29] T. Rikitake, Electromagnetism and the Earth's Interior (Elsevier, Amsterdam, 1966).

- [30] R. S. Bradley, A. K. Jamil and D. C. Mienro, The electrical conductivity of olivine of high temperatures and pressures, *Geochim. Cosmochim. Acta* 28 (1964) 1169.
- [31] H. P. Coster, The electrical conductivity of rocks and high temperatures, *Royal. Astron. Soc. Monthly Notices Geophysics Suppl.* 35 (1948) 193.
- [32] T. Nagata, T. Rikitake and M. Kono, Electrical conductivity and the age of the moon. Presented at the Thirteenth Plenary Meeting, COSPAR; Leningrad, USSR (1970).
- [33] P. Goldreich and S. J. Peale, Spin-orbit coupling in the solar system, *Astron. J.* 71 (1966) 425.
- [34] P. Goldreich and S. J. Peale, The dynamics of planetary rotation, *Ann. Rev. of Astron. and Astrophys.* 6 (1968) 287.
- [35] C. P. Sonett, Resonant spin states and the anomalous rotation of Mercury, *Comm. on Astrophys. and Space Phys.* 1 (1969) 122.

FIGURE CAPTIONS

- Fig. 1. Temperature profile for two models of Mercury. These are adapted from models calculated by Fricker and Reynolds [19] by reducing all temperatures by 100° .
- Fig. 2. Temperature of a point on the equatorial surface of a model Mercury during the planetary diurnal cycle. Daytime temperature is obtained by balance of solar input and radiative loss. Nighttime temperature is based on observation (adapted from Soter and Ulrichs [23]).
- Fig. 3. The k factor as a function of surface conductivity for various surface temperatures, excitation potentials, and thermal models. Surface temperatures are 50° , 75° and 100° C. For a given surface conductivity the k factor decreases as the temperature increases. Excitation energies are 0.5 and 0.8 eV, and the hot and warm models are as described in the text.
- Fig. 4. Ranges of σ_0 and E for given surface conductivities. The surface temperature is taken to be 75° C. Some representative conductivities are located on the plot. Points are labeled with numbers corresponding to conductivity functions in table 1. For indicated values of the saturation index k , the shaded areas indicate surface conductivities consistent with a range of thermal models. The indicated range for $k = 0.1$ separates the detectable and relatively undetectable planetary solar wind interactions. It is seen that a strong reaction could be produced by some of the materials, including the material from the lunar sample.

Fig. 5. Relative power absorbed by the unipolar generator current system as a function of k factor. The absolute power is obtained from the product of this function and parameters that depend only on the solar wind.

TEMPERATURE PROFILE FOR TWO MERCURY MODELS
(ADAPTED FROM FRICKER AND REYNOLDS)

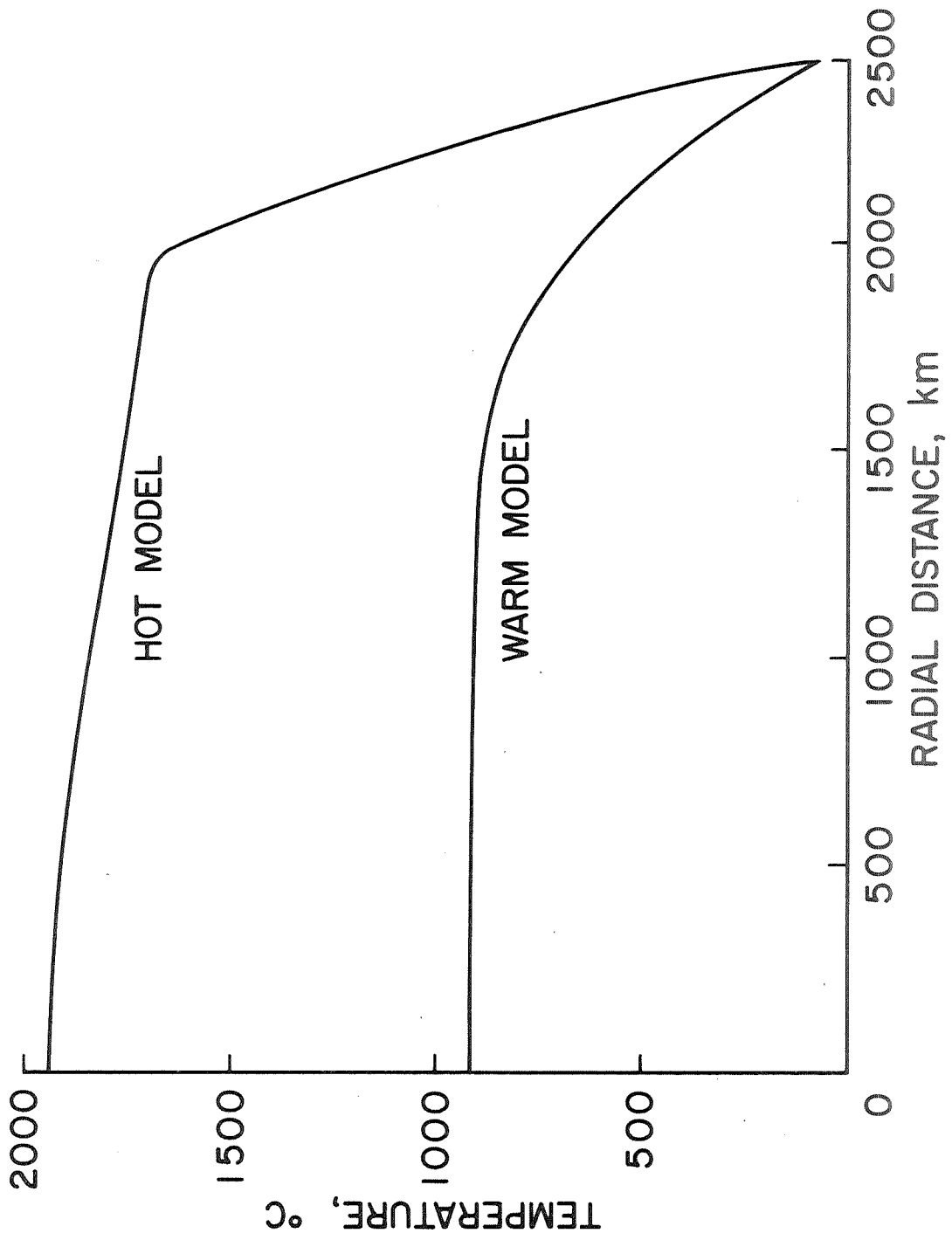


Fig. 1

EQUATORIAL SURFACE TEMPERATURE FOR MODEL MERCURY

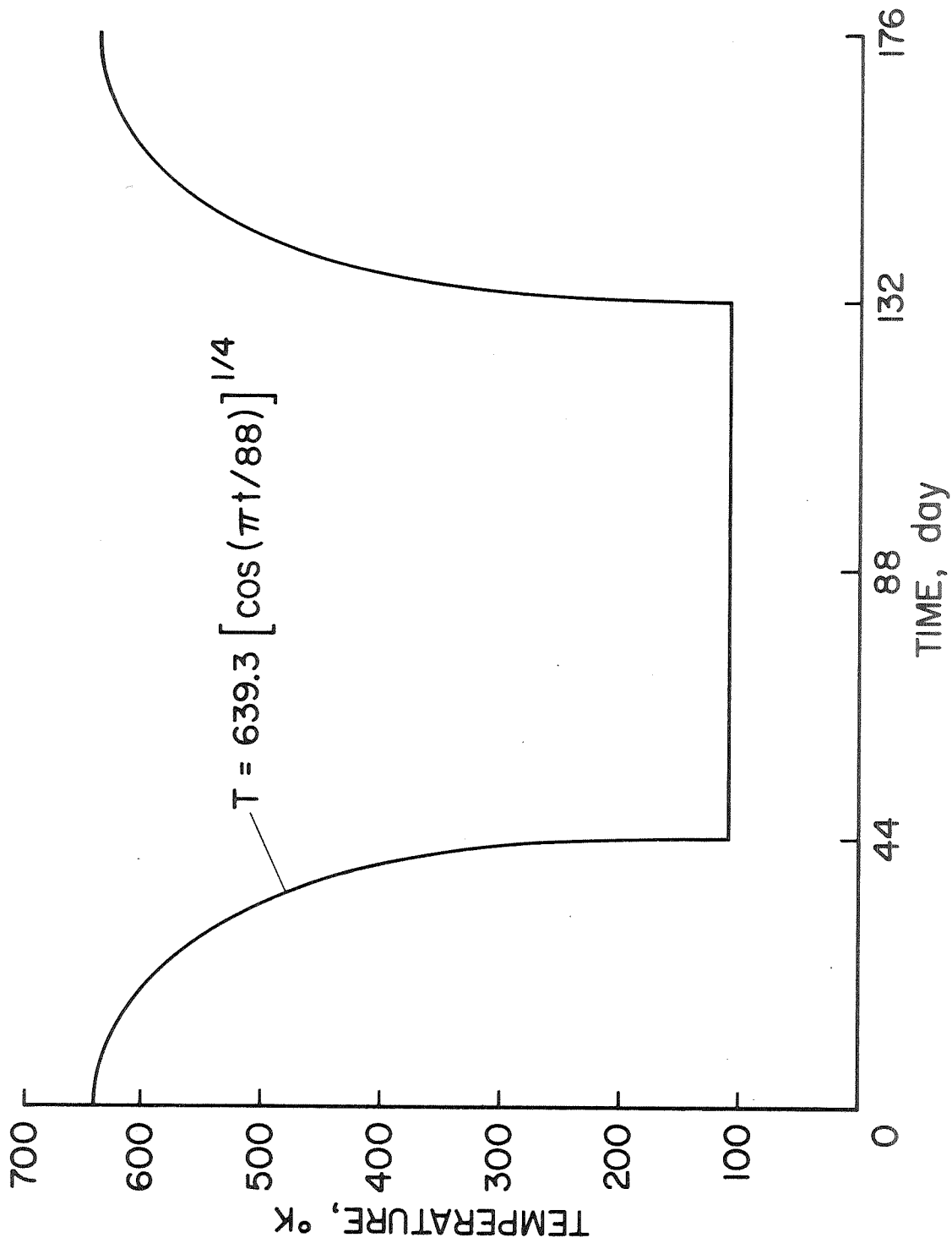


Fig. 2

K FACTOR AS A FUNCTION OF SURFACE CONDUCTIVITY

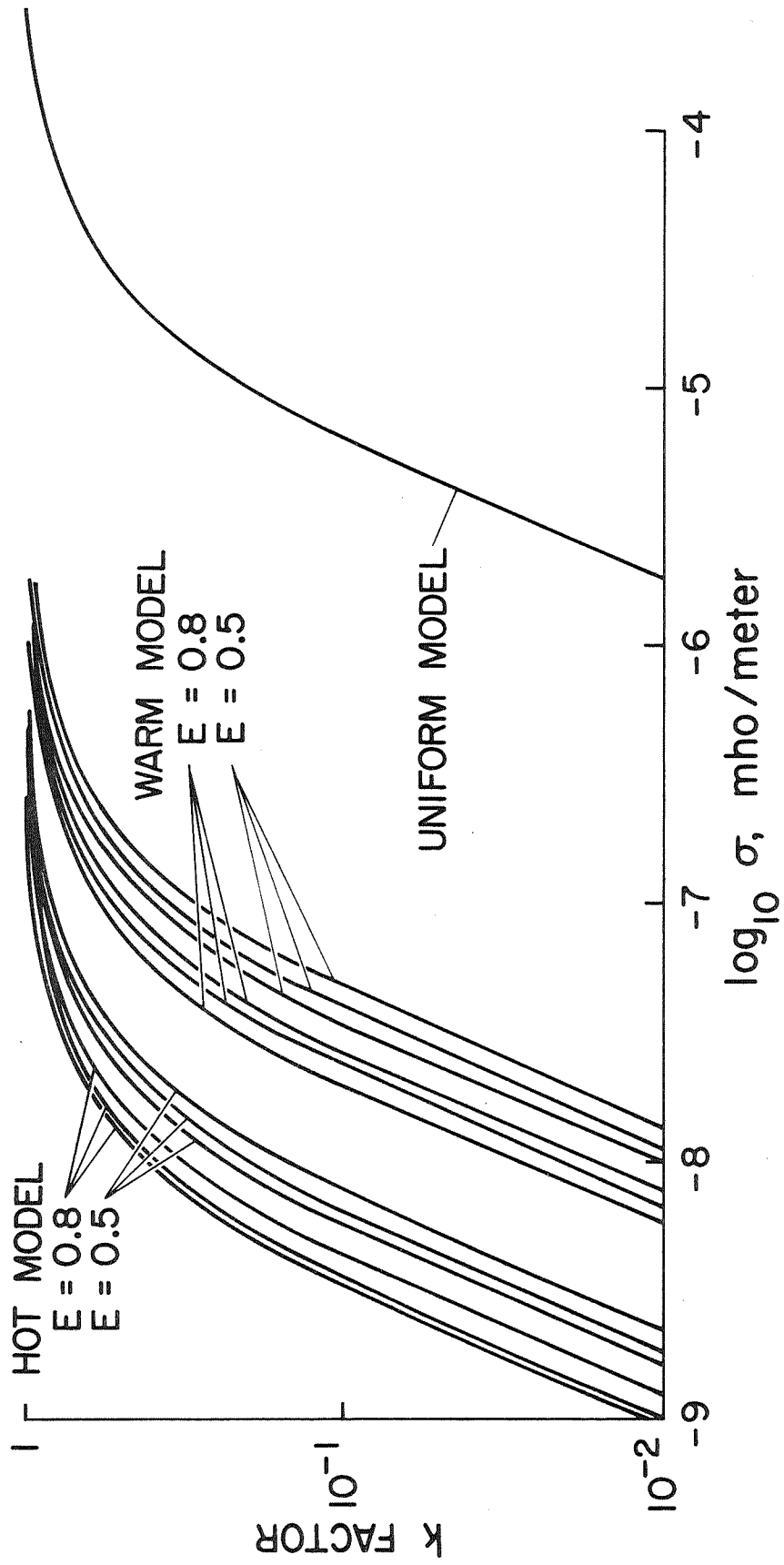


Fig. 3

σ_0 AND E AS A FUNCTION OF SURFACE CONDUCTIVITY

T = 75°C

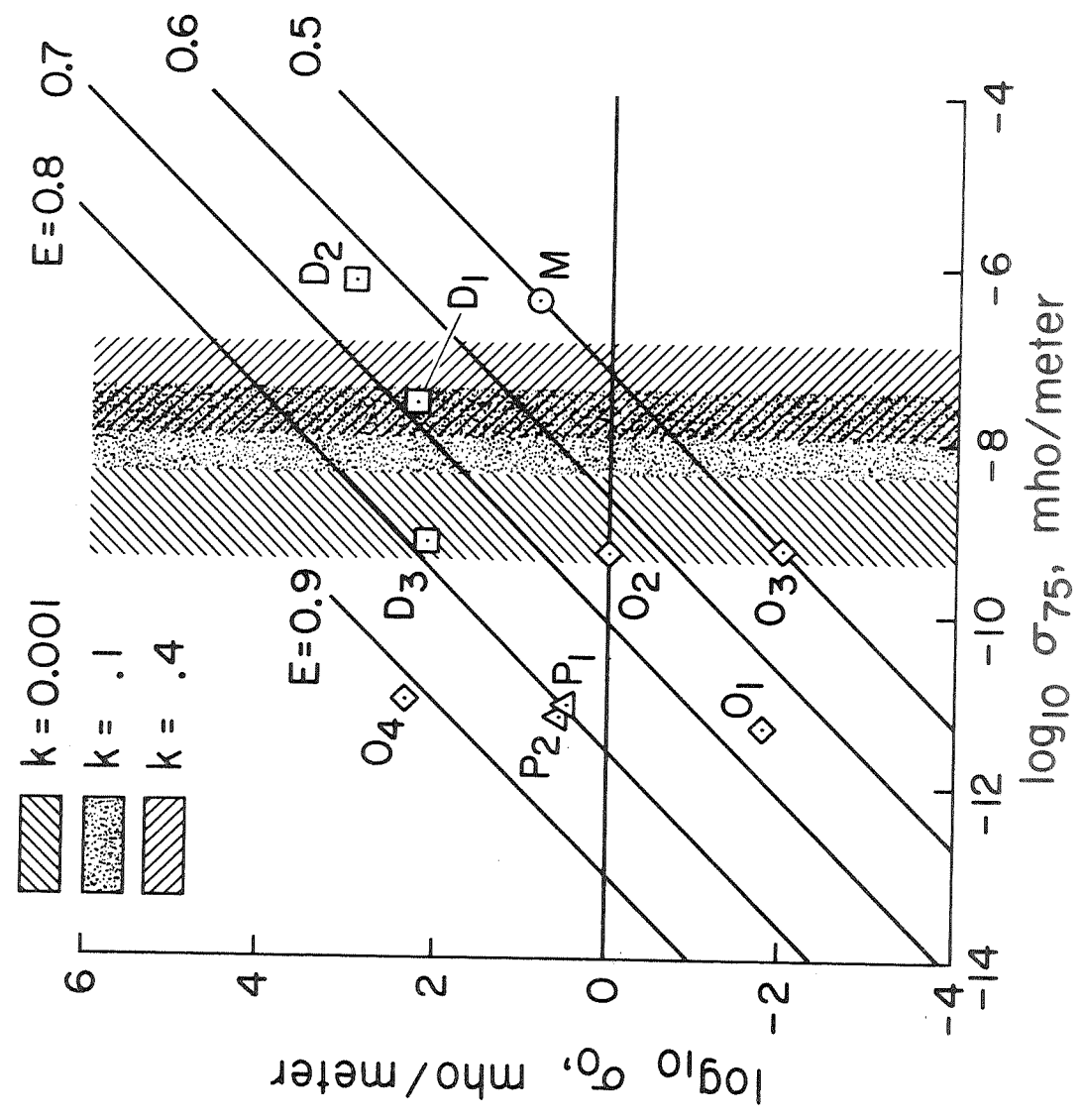


Fig. 4

RELATIVE POWER R_r AS A FUNCTION OF k FACTOR

$$R_r = 1.5 (3k)^{1/2} (1-k)$$

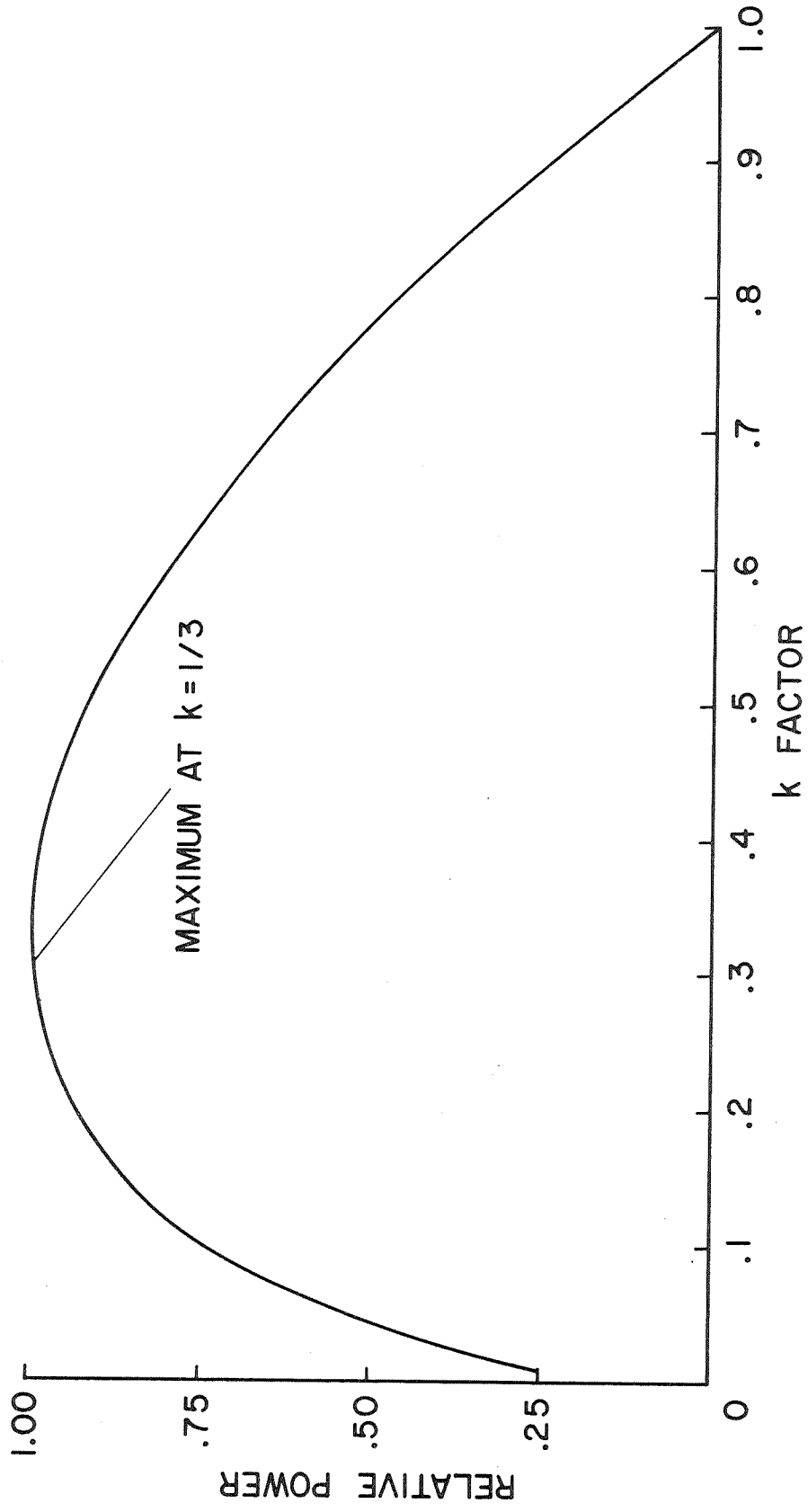


Fig. 5